COMSOL
CONFERENCE
2024 FLORENCE

Process simulation of Directed Energy Deposition process using COMSOL Multiphysics®

Vaibhav Nain[1]
1. Irepa Laser, Illkirch-Graffenstaden, France

Abstract

The process-induced deformation in the DED fabricated part is a critical issue to the scaling of the technology. An inefficient and expensive experiment trial-and-error approach is utilized to tackle this issue; however, it is not feasible for large parts. Researchers have, therefore, focused on modeling and developed several modeling strategies. Computation time remains a roadblock with these traditional models. Hence, almost no work is available in the literature focusing on large-part simulation. In the present paper, the authors develop a time-efficient simplified model capable of accurately simulating large parts employing COMSOL Multiphysics®. Heat transfer in Solids and Solid mechanics modules combined with Events interface to model the thermomechanical response of the DED fabricated part. The numerical model provides detailed insight concerning the temperature evolution and deformation in the DED part. The numerical model is successfully validated with experimental data obtained at Irepa Laser. The proposed model yields better results when compared with traditional models in terms of computation speed and accuracy. Finally, the proposed model accurately simulates an industrial part within a few hours of computation time.

Keywords: Directed energy deposition, DED, Thermomechanical simulation, Meso-scale, Macro-scale, Inherent strain, Efficient thermal cycle, ETC

1 Introduction

Directed energy deposition (DED) is an additive manufacturing (AM) process that fabricates parts by adding material layer by layer. DED uses an energy source (laser/arc) to create a melt pool onto the substrate or already-deposited layers into which feedstock material (powder/wire) is injected. The melt pool follows the pre-programmed deposition path to deposit each layer, progressively building the part layer-by-layer. During the process, with the deposition of each new layer, the substrate and already-deposited layers experience repeated and steep thermal cycles of heating and cooling. Due to these large thermal gradients, local inhomogeneous thermal strains cause distortions that negatively affect the part's dimensional accuracy. DED has the unique feature of being able to fabricate large-size parts. However, the process-induced distortion is one of the most critical challenges impeding the adoption of DED for the fabrication of large-size part [1]. Classically, distortions can be reduced by a certain magnitude with optimization of DED parameters, tool-path planning, and inter-layer dwell times [2]. Although these expensive, inefficient experimental optimizations can reduce the distortions to an extent, the problem persists [3]. Alternatively, utilizing simulation can be a better approach to overcome this issue. Several high-fidelity finite element (FE) models based on computational weld mechanics (CWM) have already been validated in the literature [4]. These meso-scale models accurately capture the thermomechanical response of the DED part, although they require enormous computation resources and high computation time for simulating a few layers [5]. Hence, they are limited to small parts and are impractical for large-part simulations.

Computation time is the primary reason hindering the development of a digital tool for the industry; however, very few works have been found in the literature focusing on this aspect. Some researchers have developed multi-scale models that simulate real-size parts by reducing computation time. The multi-scale methods employed in the literature are divided into two categories: (1) Flash heating (FH) method and (2) Inherent strain-based (IS) method. The FH method does not consider the local deposition pattern. The model simplifies it by numerically depositing and heating each layer or group of layers (macro layer) with each time step. This is repeated until the complete part is digitally fabricated in a layer-by-layer approach. Some researchers have effectively employed the FH method for real-part DED simulation[6], [7], [8]. However, computation accuracy was a problem in its current simplified form. Therefore, the FH method was further refined, accounting for the deposition sequence by decomposing each layer into several sub-domains and sequentially heating (SFH) them [9]. Few researchers have demonstrated its application for real-parts DED simulation, yielding accurate results with a speed-up by a factor of 5-20 compared with meso-scale models [10], [11], [12]. However, the SFH method cannot be used for large-size parts as the computation time is still high.

The "inherent strain" (IS) is extracted in the IS method by performing the local-level meso-scale thermo-mechanical simulation over a small domain

of the complete part. Then, the calculated IS is applied as an initial strain (layer-by-layer) to the quasi-static mechanical analysis of the whole part. The IS method has been extensively validated for powder bed fusion AM methods but does not work for the DED as the part scale differs. Therefore, the modified IS (MIS) method is developed for single-walled DED structures [13]. The MIS method yielded accurate results and achieved a speed-up by a factor of 20 compared to traditional meso-scale models. However, the author states that the MIS works only for small, simple-walled DED structures. The MIS method still requires much development before its validation for real-size parts.

This study develops a time-efficient FE model capable of simulating large parts. The proposed model employs the FH method, whereby the newly deposited macro layer is heated for a pre-defined heating and cooling period, strictly following energy conservation in simulation. The effect of layer lumping on the simulation performance is presented. The simulation results are successfully compared with the in-situ experimental data. The numerical model demonstrated its capability to simulate an industrial part within a few hours.

2 Experimental Set-Up

The experiment (EXP) was done with an in-house-developed laser-powder DED machine equipped with a 2kW diode laser and a coaxial powder nozzle. An SS 316L rectangular sample of 100 layers was fabricated on the substrate (S235 steel) with the CAD schematic shown in Figure 1. The associated process parameters are provided in Table 1.

Table 1: Process parameters of the EXP

Process parameter	Value
Laser spot size & power	2.2 mm & 800 W
Laser travel speed	1 m/min
No. of tracks per layer	2
Width (2 tracks) × Layer height	3.7 × 0.45 mm

Cantilever tooling was employed to fix the substrate from one end and allow it to move from the other, as highlighted in red in Figure 1. The Laser Displacement Sensor (LDS) captures in-situ distortion from the free end, and thermocouples record the in-situ temperature at the substrate's bottom face, as shown in Figure 1 (bottom).

3 Numerical Model

The FE model is developed using COMSOL Multiphysics® software. Heat transfer and solid mechanics modules model the part's thermomechanical response. The events interface models the laser on-off, i.e., FH and cooling. The numerical model performs sequential simulations: first, a transient thermal analysis to obtain the

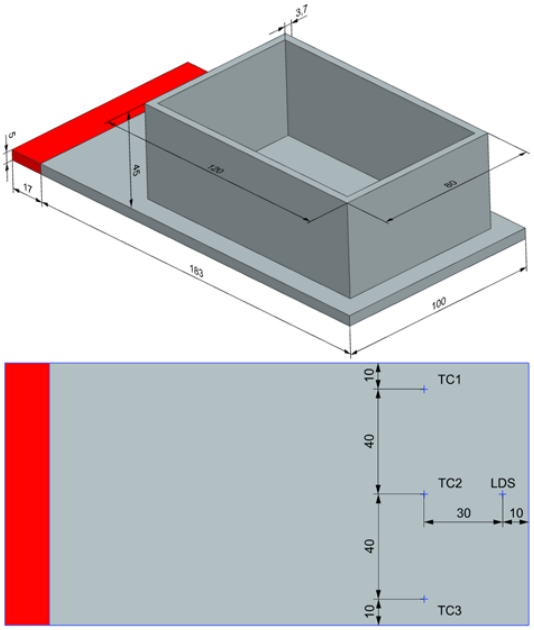

Figure 1: CAD schematic (Top) and sensors locations at the substrate's bottom surface (Bottom)

temperature fields. The thermal results are then fed as an input for a quasi-static mechanical analysis, which predicts the mechanical response. A Multiphysics thermal expansion interface links sequentially coupled simulations.

3.1 Transient thermal analysis

The governing transient heat transfer differential equation calculates temperature (T) as a function of time (t)over a Lagrangian domain Ω.

$$\rho(T)c_p(T)\frac{\partial T}{\partial t} = -\nabla \cdot \boldsymbol{q}(\boldsymbol{r},t) + Q(\boldsymbol{r},t) \quad (1)$$

where ρ(T) and c_p(T) is the temperature-dependent density and specific heat capacity, respectively. Q is the heat flux, and q is the heat flux vector, given as:

$$\boldsymbol{q} = -k(T)\nabla T \quad (2)$$

k is the material's thermal conductivity. The material is numerically deposited using a layer-by-layer approach (FH). The actual deposition time for each layer t_{layer} is decomposed into two time intervals i.e., heating (t_{heat}) and cooling (t_{cool}). Upon activating the complete macro-layer, a volumetric heat flux (Q) is applied for t_{heat} period following the energy conservation rule [14].

$$Q = \frac{A \cdot P}{V_{layer}} \cdot \frac{t_{layer}}{t_{heat}} \cdot l_f \quad (3)$$

A is heat source absorption, V_{layer} is the volume of the layer, l_f is the layer lumping factor/size, and t_{heat} is calculated as follows:

$$t_{heat} = h_f \frac{\phi_L}{v_L} \quad (4)$$

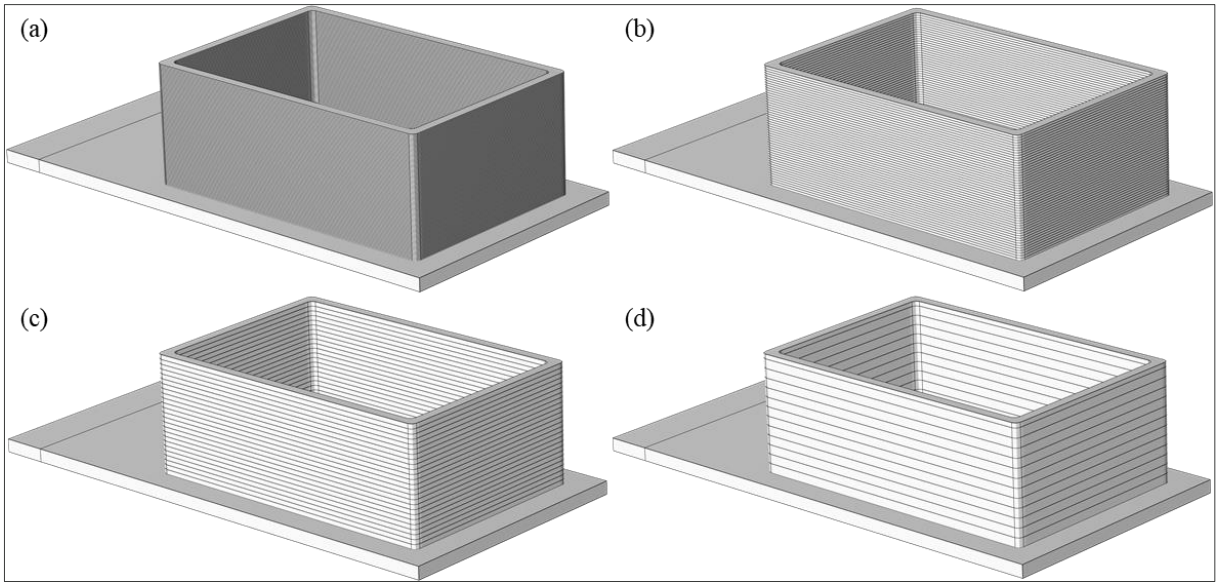

Figure 2: Impact of layer lumping factor (l_f) on macro layer height (Δz_t) (a) No lumping (b) 2-layer (c) 4-layer (d) 8-layer

h_f is the heat scaling factor whose value is 7 for all simulations. Following the heating period, the layer can cool down for the t_{cool} period. To account for convective and radiative heat losses in the model, the following boundary conditions are applied on all surfaces, using Newton's and Stefan-Boltzmann law, respectively:

$$q_{loss} = h(T_s - T_{amb}) + \varepsilon\sigma(T_s^4 - T_{amb}^4) \quad (5)$$

With h, the convective heat transfer coefficient in (W/m^2K), T_s is the surface temperature, and T_{amb} is the ambient temperature, i.e., 20°C, ε is the surface emissivity, and σ is the Stefan–Boltzmann constant.

3.2 Mechanical analysis

The mechanical analysis is based on an elastoplastic formulation considering isotropic non-linear material hardening. The governing mechanical stress equilibrium where σ denotes the stress tensor is:

$$\nabla.\sigma = 0 \quad (6)$$

The mechanical constitutive law is:

$$\sigma = C\varepsilon_e \quad (7)$$

C is the stiffness tensor. Considering small-strain deformation theory, total strain (ε) is decomposed additively in elastic (ε_e) and inelastic part (ε_{in}):

$$\varepsilon = \varepsilon_e + \varepsilon_{in} \quad (8)$$

The thermal (ε_{th}) and plastic strains (ε_{pl}) are included in the inelastic strain:

$$\varepsilon_{in} = \varepsilon_{th} + \varepsilon_{pl} \quad (9)$$

The thermal strain is calculated using the coefficient of thermal expansion (α):

$$\varepsilon_{th} = \alpha\left(T - T_{ref}\right) \quad (10)$$

The plastic strain is calculated by enforcing the Von-Mises yield criterion:

$$F = \sigma_{vm} - \sigma_y\left(\varepsilon_{eq}, T\right) \leq 0 \quad (11)$$

F is the yield function, σ_{vm} is Von-Mises's stress, and ε_{eq} is the equivalent plastic strain. σ_y is the yield stress, which is calculated by:

$$\sigma_y\left(\varepsilon_{eq}, T\right) = \sigma_{y0}(T) + \sigma_{sat}\left(1 - e^{-\beta\varepsilon_{eq}}\right) \quad (12)$$

σ_{y0} is the initial yield stress, σ_{sat} is saturation flow stress, and β is saturation exponent. In the model, Voce hardening law is used to model non-linear hardening. Temperature-dependent material properties such as k, c_p, Young's modulus (E), σ_y, α are taken from the literature [5]. To model clamping conditions, a fixed boundary condition is imposed on the highlighted surfaces in red (Fig. 1).

3.3 Layer lumping

A group of layers is merged/lumped together to form a "macro layer." As the number of layers lumped together increases, the height/thickness of the macro layer (Δz_t) increases, as shown in Figure 2. Layer lumping aims to reduce the computation time by decreasing the number of computation time steps, coarser mesh elements, etc. However, the effect of Δz_t on computation accuracy and time still needs to be investigated for DED. This work considers four different configurations, as shown in Table 2.

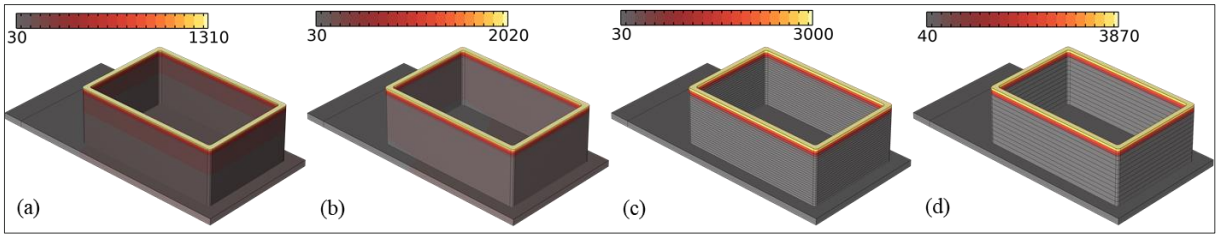

Figure 3: Effect of layer lumping on peak temperature (a) No lumping (b) 2-layer (c) 4-layer (d) 8-layer

Table 2: Layer lumping configurations and simulation parameters used in this study

Sim. parameters	Lumping Configuration (l_f)			
	1 (No)	2	4	8
Macro layers	100	50	25	13
Δz_t (mm)	0.45	0.9	1.8	3.6
Mesh elements	58970	37136	32203	28305

3.4 Material deposition model

Layers are numerically deposited employing the "quiet element" method. The computation domain consists of the substrate and the part from the beginning of the analysis. Dummy material properties are assigned to the quiet elements, i.e., the fabricated part, so they do not negatively affect the numerical results.

$$k_{quiet} = 0.001\ (W/(m.K)) \quad (13)$$

$$E_{quiet} = 1\ (GPa) \quad (14)$$

The material properties switch from dummy to metal properties as the 1st layer is activated following the activation criterion. The process of layer activation is repeated until the complete part is numerically deposited.

3.5 Numerical implementation

MUMPS and the Suggested Direct Solver were employed for thermal and mechanical simulations. The time-stepping formulation was set to be "strict" and coupled with an events interface, making it reliable to avoid skipping t_{heat} period (0.132 s) followed by the t_{cool} period (function of Δz_t) for each macro layer. Irrespective of Δz_t, one and two-time steps are taken for the t_{heat} and t_{cool} periods in the thermal analysis for each macro-layer.
CAD simplification is done by taking constant width and height dimensions for all layers. The author has previously fabricated different geometries (simple walls) using the same materials (SS 316L) and process parameters in the same DED machine [11]. Therefore, the values for laser absorptivity, emissivity, convection coefficient, and forced convection coefficient are kept the same in this study. The simulations were performed on a workstation with 16 cores, 128 GB RAM, and an Intel Xeon W-2275 processor.

4 Results and discussion

4.1 Thermal history

Thermal analysis is successfully done as Figure 3 shows the last layer's simulated peak temperatures (orange) during the macro-layer's heating phase (t_{heat}). *The peak temperatures increase with increased Δz_t as more energy is deposited during the t_{heat} with increased lumping. The far-field temperature magnitude at the TC location decreases with increased Δz_t, as observed in Figure 4*. Even though a significant mismatch in temperature magnitude can be observed in Figure 4, the numerical model captures the trends. However, the difference becomes important with a higher value of Δz_t (8-layer). Globally, the temperature history of the fabricated sample is kept similar to the experiment by applying cooling times (t_{cool}) after the heating (t_{heat}) corresponding to the time it would take the laser to finish the macro-layer, strictly following the energy conservation.

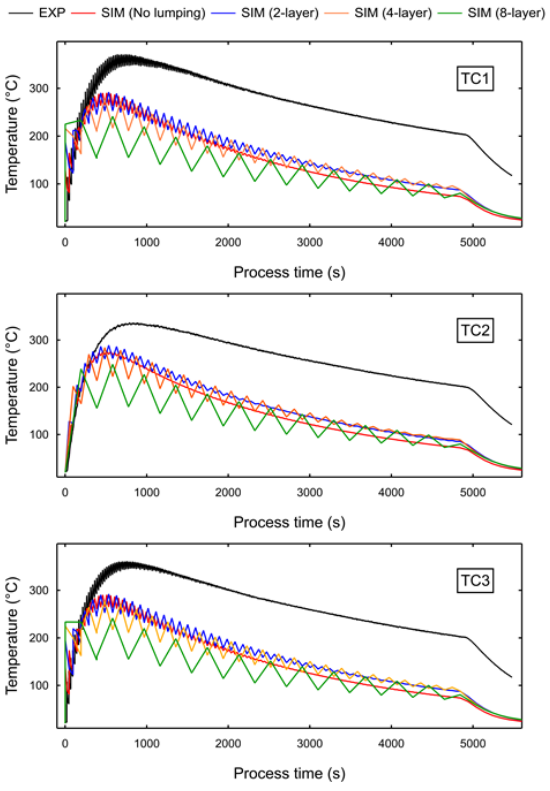

Figure 4: Calculated in-situ thermal history at TC location for all cases

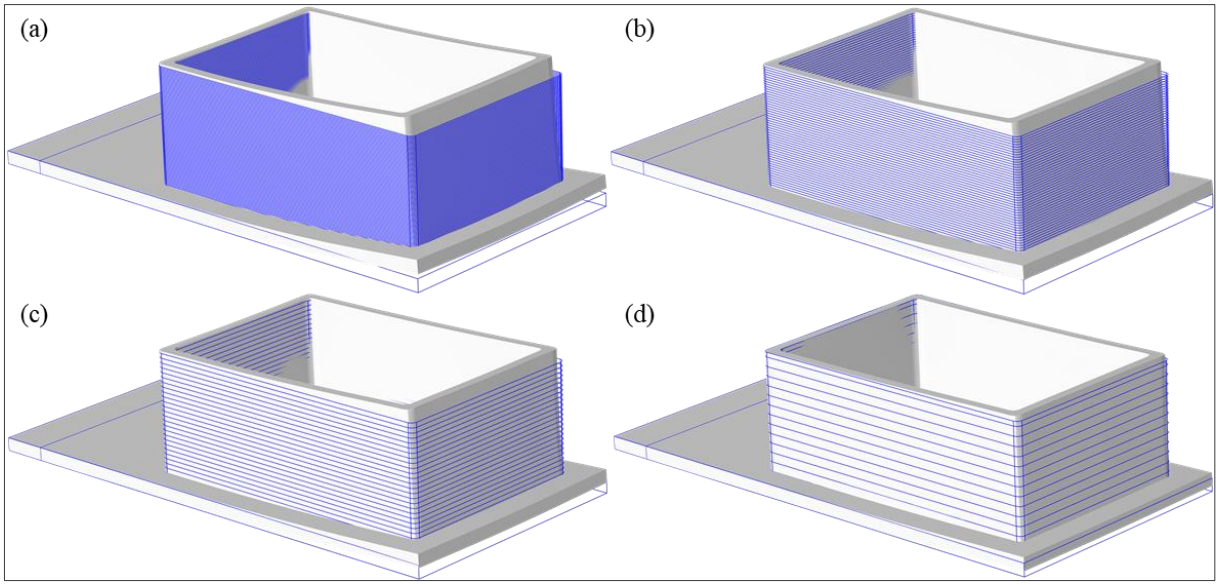

Figure 5: Mechanical model showing final distorted shape of the sample (a) No lumping (b) 2-layer (c) 4-layer (d) 8-layer

4.2 Mechanical history

Figure 5 shows the final distortion of the SS 316L sample for all cases. Figure 6 shows a significant mismatch of predicted distortions at the LDS location after depositing the first 30 layers. This is due to the FH method's simplification, whereby the moving heat source is not modeled, and local temperatures are not captured. However, the FH method's calculated distortion (no lumping) agrees well with in-situ experimental data during the metal deposition at the remaining layers and cooling phase. As discussed previously, an increase in Δz_t results in fewer heating-cooling cycles of lower temperature magnitude at far-field temperatures, resulting in lower thermal train values yielding lesser distortion magnitude. This trend can be observed in Figure 6. However, the lumping model accurately captures the distortion trends. This is further validated by the final distortion values at the LDS location predicted by the model, which are presented in Table 3.

Table 3: Final distortion value at LDS location

Final z-distortion (mm)	LDS location
Experimental	3.88
No-lumping simulation	4.83
2-layer lumping simulation	3.65
4-layer lumping simulation	2.89
8-layer lumping simulation	1.53

Employing the layer lumping method drastically reduces calculation time and the number of time steps, as presented in Figure 7. The 2-layer model reduces computation time from 5.4 h (reference: no lumping) to 1.25 h. With the 8-layer model, run time is reduced by a factor of 25. However, a compromise has to be made between computation accuracy and time, as a higher value of Δz_t results in a loss of accuracy. The results agree well with the experimental reference data. However, the effect of layer lumping on different part designs and materials needs to be studied in detail. Also, identifying an optimized layer lumping size without significantly

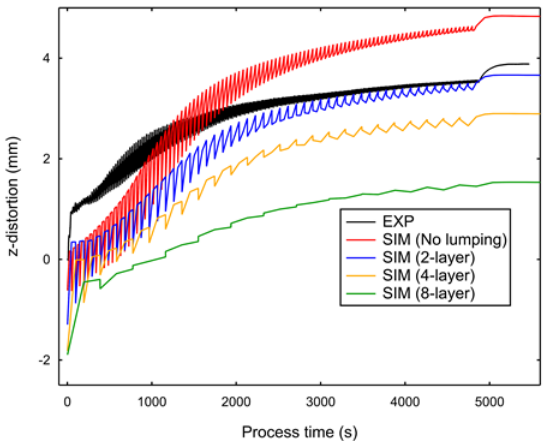

Figure 6: Calculated in-situ distortion results at LDS location for all cases

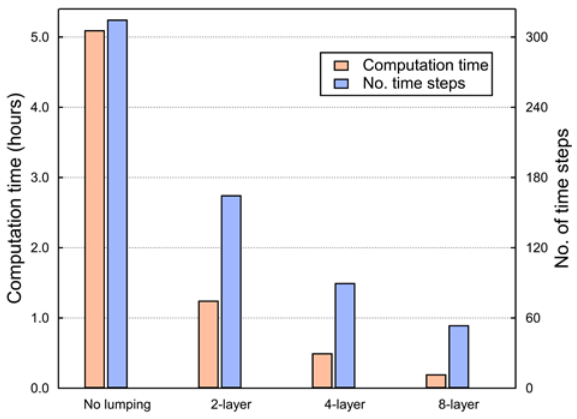

Figure 7: Computation performance: Comparison of computation time and time steps for all cases

compromising accuracy is critical. Finally, the effect of heating phase duration (t_{heat}) on part response should be investigated. A detailed investigation will be done to carry out these tasks in the future.

5 Conclusions

The proposed FH method reduces computation times for DED process simulation by simplifying the deposition strategy. The predicted results are close to the experimental data with acceptable computation time. FH with a layer lumping model further reduces computation time while maintaining an adequate level of accuracy. The model provides the unique capability to simulate large-size industrial parts within a few hours. Moreover, the proposed simplified numerical model can be easily adapted to commercially available software. We are developing a fully automated COMSOL App for large-part DED simulation.

References

[1] W. Oropallo and L. A. Piegl, "Ten challenges in 3D printing," *Engineering with Computers*, vol. 32, no. 1, pp. 135–148, Jan. 2016, doi: 10.1007/s00366-015-0407-0.

[2] E. R. Denlinger, J. C. Heigel, P. Michaleris, and T. A. Palmer, "Effect of inter-layer dwell time on distortion and residual stress in additive manufacturing of titanium and nickel alloys," *Journal of Materials Processing Technology*, vol. 215, pp. 123–131, Jan. 2015, doi: 10.1016/j.jmatprotec.2014.07.030.

[3] W. E. Frazier, "Metal Additive Manufacturing: A Review," *J. of Materi Eng and Perform*, vol. 23, no. 6, pp. 1917–1928, Jun. 2014, doi: 10.1007/s11665-014-0958-z.

[4] M. Bayat, W. Dong, J. Thorborg, A. C. To, and J. H. Hattel, "A review of multi-scale and multi-physics simulations of metal additive manufacturing processes with focus on modeling strategies," *Additive Manufacturing*, vol. 47, p. 102278, Nov. 2021, doi: 10.1016/j.addma.2021.102278.

[5] M. Biegler, B. Graf, and M. Rethmeier, "In-situ distortions in LMD additive manufacturing walls can be measured with digital image correlation and predicted using numerical simulations," *Additive Manufacturing*, vol. 20, pp. 101–110, Mar. 2018, doi: 10.1016/j.addma.2017.12.007.

[6] K. Babkin, E. Zemlyakov, S. Ivanov, A. Vildanov, I. Topalov, and G. Turichin, "Distortion prediction and compensation in direct laser deposition of large axisymmetric Ti-6Al-4V part," *Procedia CIRP*, vol. 94, pp. 357–361, Jan. 2020, doi: 10.1016/j.procir.2020.09.145.

[7] G. Turichin, E. Zemlyakov, K. Babkin, S. Ivanov, and A. Vildanov, "Analysis of distortion during laser metal deposition of large parts," *Procedia CIRP*, vol. 74, pp. 154–157, Jan. 2018, doi: 10.1016/j.procir.2018.08.068.

[8] K. Salonitis, L. D'Alvise, B. Schoinochoritis, and D. Chantzis, "Additive manufacturing and post-processing simulation: laser cladding followed by high speed machining," *Int J Adv Manuf Technol*, vol. 85, no. 9, pp. 2401–2411, Aug. 2016, doi: 10.1007/s00170-015-7989-y.

[9] Y. Zhang, G. Guillemot, M. Bernacki, and M. Bellet, "Macroscopic thermal finite element modeling of additive metal manufacturing by selective laser melting process," *Computer Methods in Applied Mechanics and Engineering*, vol. 331, pp. 514–535, Apr. 2018, doi: 10.1016/j.cma.2017.12.003.

[10] J. Wang, J. Zhang, L. Liang, A. Huang, G. Yang, and S. Pang, "A line-based flash heating method for numerical modeling and prediction of directed energy deposition manufacturing process," *Journal of Manufacturing Processes*, vol. 73, pp. 822–838, Jan. 2022, doi: 10.1016/j.jmapro.2021.11.041.

[11] V. Nain, T. Engel, M. Carin, and D. Boisselier, "Conventional Meso-Scale and Time-Efficient Sub-Track-Scale Thermomechanical Model for Directed Energy Deposition," *Materials*, vol. 15, no. 12, Art. no. 12, Jan. 2022, doi: 10.3390/ma15124093.

[12] M. Biegler, B. A. M. Elsner, I. Neubauer, J. Lemke, and M. Rethmeier, "Result quality evaluation of Directed Energy Deposition Additive Manufacturing simulations with progressive simplification of transient heat-source motion," *Procedia CIRP*, vol. 111, pp. 277–281, 2022, doi: 10.1016/j.procir.2022.08.021.

[13] X. Liang, L. Cheng, Q. Chen, Q. Yang, and A. C. To, "A modified method for estimating inherent strains from detailed process simulation for fast residual distortion prediction of single-walled structures fabricated by directed energy deposition," *Additive Manufacturing*, vol. 23, pp. 471–486, Oct. 2018, doi: 10.1016/j.addma.2018.08.029.

[14] Y. Zhang, G. Guillemot, M. Bernacki, and M. Bellet, "Macroscopic thermal finite element modeling of additive metal manufacturing by selective laser melting process," *Computer Methods in Applied Mechanics and Engineering*, vol. 331, pp. 514–535, Apr. 2018, doi: 10.1016/j.cma.2017.12.003.